NANO · MICRO small
www.small-journal.com

Hybrid Multimaterial 3D Printing Using Photocuring-While-Dispensing

*Jie Jin, Fangzhou Zhang, Yulong Yang, Chengqian Zhang, Haidong Wu, Yang Xu, and Yong Chen**

Three-dimensional (3D) printing methods, such as vat photopolymerization (VPP) and direct-ink-writing (DIW) processes, are known for their high-resolution and multimaterial capabilities, respectively. Here a novel hybrid 3D printing technique that combines the strengths of VPP and DIW processes to achieve multimaterial and high-resolution printing of functional structures and devices, is presented. The method involves dispensing liquid-like materials via syringes into a photocurable matrix material and subsequently using a Galvano mirror-controlled laser beam to selectively photocure the dispensed material trace or the matrix material surrounding the trace. The laser beam scanning and syringe dispensing are synchronized with a set delay to control liquid diffusion and in situ fixture. The versatility of the method is demonstrated by fabricating intricate 3D ant and wheel prototypes using various materials available for VPP and DIW technologies. The proposed photocuring-while-dispensing strategy offers advantages over conventional multimaterial 3D printing methods, such as integrating materials regardless of photocurability and viscosity, and fabricating heterogeneous structures with complex geometries and high resolution. With its principle demonstrated, this multimaterial 3D printing process will open up a wide range of potential applications with diverse functionalities and materials.

1. Introduction

The ability to build three-dimensional (3D) structures using various material compositions has the potential to drive scientific advances in multiple areas,[1–5] such as tissue engineering,[6,7] soft robotics,[8,9] wearable devices,[10,11] and others. Multimaterial 3D printing that can fabricate functional structures and devices composed of heterogeneous materials in the same part has attracted increasing attention.[12,13] While multijet modeling (MJP) is the most widely used multimaterial 3D printing process,[14,15] the micronozzle-based ink-jetting mechanism limits its material selection to liquids with low viscosity, hindering broader applications. Another 3D printing method, direct ink writing (DIW), can dispense a wide variety of materials, such as bio-inks,[16,17] conductive inks,[10] and magnetized fluids,[18–22] and multiple syringes to achieve multimaterial 3D printing can easily be integrated into a DIW system.[23,24] In addition to selectively dispensing various materials in desired positions, the *Y*-type channels and fluidic mixing devices have been designed for DIW-based multimaterial 3D printing to mix multiple materials and extrude the mixed fluid through the nozzle tip.[25–27] However, a significant drawback of the DIW-based printing method is its relatively slow printing speed due to the required mechanical movements. Also, maintaining the shape of the dispensed material when it comes out of the nozzle tip has been challenging, particularly when dispensing around the boundary of the building layers. As a result, the DIW materials need to be formulated with shear thinning

J. Jin, Y. Xu, Y. Chen
Center for Advanced Manufacturing
University of Southern California
Los Angeles, CA 90007, USA
E-mail: yongchen@usc.edu
J. Jin, Y. Xu, Y. Chen
Daniel J. Epstein Department of Industrial and Systems Engineering
University of Southern California
Los Angeles, CA 90089, USA
The ORCID identification number(s) for the author(s) of this article can be found under https://doi.org/10.1002/smll.202302405

DOI: 10.1002/smll.202302405

F. Zhang, Y. Chen
Department of Aerospace and Mechanical Engineering
University of Southern California
Los Angeles, CA 90089, USA
Y. Yang
Mork Family Department of Chemical Engineering and Materials Science
University of Southern California
Los Angeles, CA 90089, USA
C. Zhang
School of Mechanical Engineering
Zhejiang University
Hangzhou, Zhejiang 310027, China
H. Wu
School of Electromechanical Engineering
Guangdong University of Technology
Guangzhou, Guangdong 510006, China

properties to avoid flowing down to the previous layers.[21] In comparison, vat photopolymerization (VPP), aka stereolithography apparatus (SLA), has been well known as a high-speed, high-accuracy, and high-definition printing method using ultraviolet (UV) light controlled by a laser or a digital light processing (DLP) device to photocure liquid resin.[28,29] While multimaterial 3D printing based on VPP has been reported by switching between different material reservoirs,[30–33] changing materials between liquid resin vats is a significant challenge. Additional procedures required in the printing process, such as rinsing the uncured material attached to the cured layers and drying the rinsed surface afterward, lead to significant time and material waste. In addition, many nonphotocurable yet functional materials cannot be used in VPP.

Several successful attempts have been made to develop a hybrid 3D printing approach by combining the VPP and DIW methods.[34–36] Rau et al. presented an integrating method that uses DIW to print high-viscosity photopolymer resins aided by using VPP to define its boundary shape.[34] Peng et al. presented a hybrid approach by integrating VPP and DIW to print multimaterial structures.[35,36] So far, the developed hybrid methods have used the top-down projection configuration, in which the DIW materials are extruded on the top surface of the VPP layers in the air. The DIW materials are specially formulated to avoid flowing down to the previous layers since the air cannot support the extruded DIW liquid. However, some recent DIW studies have shown that using a syringe nozzle tip to dispense a material inside another gel-like matrix material can retain the shape of the dispensed material, prevent it from collapsing due to surface tension, and enable dispensing in a 3D space.[10,37,38] Meanwhile, the surrounding gel-like material can work as supporting material, making it possible for a DIW process to dispense material in a 3D space rather than just on a two-dimensional (2D) plane.[39,40] These findings have motivated us to investigate a new hybrid 3D printing strategy by directly immersing the DIW nozzle tips in a photocurable resin reservoir so functional materials can be directly dispensed and fixed at the desired position inside the matrix material. A critical challenge to be addressed here is controlling the diffusion between the DIW and VPP liquids and in situ bonding the DIW material with the VPP material during the layer-based printing process.

Here we use the bottom-up VPP configuration to allow the laser beam's unblocked access to the extruded material traces during the printing process. **Figure 1** shows the principle of the developed hybrid 3D printing approach that integrates two broadly accessible additive manufacturing (AM) technologies in a single printing system. This hybrid printer comprises a bottom-up VPP printer and a three-axis DIW printer. We immerse the dispense nozzle tips in a matrix material reservoir containing a photocurable resin to dispense functional materials inside the matrix material. At the same time, a UV laser scanning system is mounted below the material reservoir. Guided by the Galvano mirror, the laser beam can dynamically scan the image pattern on the base surface of the material reservoir. For each layer, the nozzle tip dispenses the material while the laser is tracing behind the nozzle tip toolpath with a set delay to photocure the newly dispensed photocurable or in situ fix the nonphotocurable materials inside the matrix material (Figure 1a,b). After photocuring the matrix material in the surrounding area, the dispensed material will stick to the substrate film of the material reservoir or the matrix material, as shown in Figure 1f. Then, a building platform will be switched to the place above the current dispensed layer and lowered down to the position where a layer thickness gap is formed between the previously built layers and the base surface of the material reservoir (Figure 1d). After an exposure of the currently built layer using a mask projection image or a scanning laser,[41] the current layer with both DIW and VPP materials will bond to the previously built layers and separate from the bottom film. This process is repeated layer by layer until all the layers of the 3D part are built.

This multimaterial 3D printing process is built on two low-cost and widely available technologies, vat photopolymerization and direct ink writing, to fabricate complex heterogeneous structures and functional devices. It can prevent DIW's material-collapsing and VPP's cross-contamination issues in multimaterial 3D printing. In the prototype hybrid system, we used a standard laser-based VPP system, while a hybrid VPP system with both a laser and a DLP system[41] can also be used to achieve a faster building process. Also, we used a low-cost pneumatically controlled dispensing system to achieve quick response and accurate material deposition (Figure S1 in the Supporting Information), while more advanced material extrusion systems can also be used.[9–11] Here the dispensers are pneumatically driven by preconfigured air pressure, and programmed valves can selectively activate each of them. Different dispensers with different nozzle diameters and air pressures may be required for the loaded DIW materials with different viscosity. We tested the prototype system with photocurable and nonphotocurable materials on its capability to engineer highly complex composites with various functionalities. This hybrid 3D printing method is versatile and could be extended to more functional materials developed for VPP and DIW technologies. It is especially suitable for printing a high-resolution structural part with small amounts of functional materials embedded inside it.

2. Results and Discussion

2.1. Characterization of Multimaterial Diffusion

The hybrid 3D printing method using photocuring-while-dispensing involves dispensing the DIW material from the nozzle tip in a photocurable liquid resin and scanning the matrix material of liquid resin using a laser beam with a set delay. During the layer printing process, the nozzle tip is immersed in the liquid matrix material, which immediately self-heals after being sheared by the dispensing nozzle, leaving no voids in the matrix material.[42,43] While dispensing target materials inside the matrix material has several advantages, a potential issue with this hybrid strategy is the diffusion of two liquids when the DIW material interacts with the VPP matrix material, resulting in defects in the designed geometry or material cross-contamination. Consequently, the width of the dispensed trace may expand toward the interface due to the diffusion effect and lose the sharp boundary between the dispensed and matrix materials (**Figure 2**a). Different liquid materials have varying diffusion

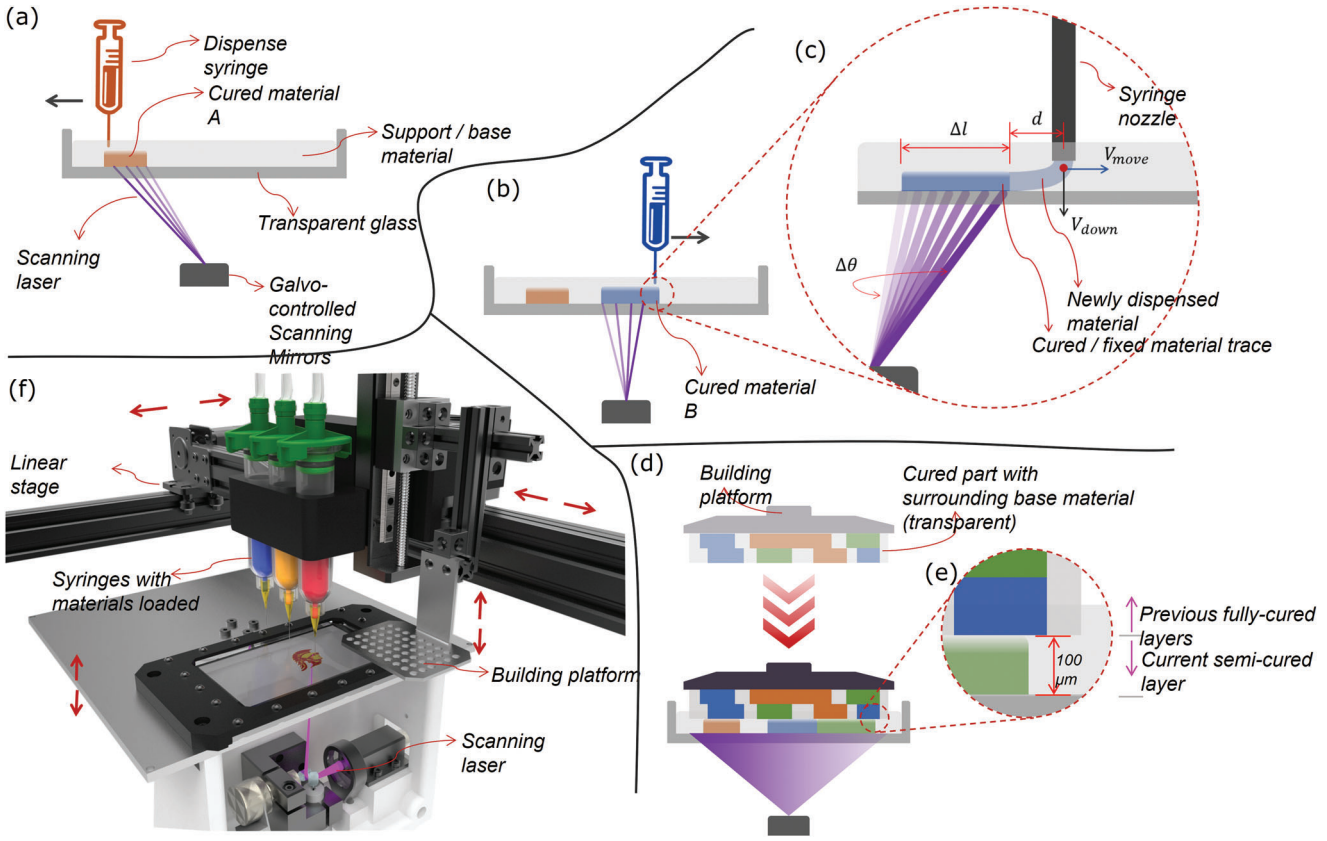

Figure 1. Schematics of the hybrid multimaterial 3D printing system based on vat photopolymerization and direct ink writing. a) First step: a dispensing syringe moves horizontally toward the left to dispense the loaded material *A* onto the bottom surface of a tank, which contains photocurable liquid matrix material. The scanning laser spot traces the dispensed material with a delay to solidify it while the syringe continues dispensing the material. b) Second step: switch to another dispensing syringe to deposit material *B*. c) A region of interest (ROI) in (b) to illustrate the photocuring-while-dispensing process in detail. d) Third step: switch to the building platform to transfer the newly built layer from the tank's bottom surface to the previously built layers with a second light exposure. e) An ROI in (d) illustrates how the current layer attaches to the previous fully cured layers. f) The designed experimental setup consists of the multimaterial DIW printhead with multiple nozzles that can move in the *XY* plane, the laser scanning-based VPP module that can scan in the *XY* plane and move in the *Z* direction, and the building platform that can move in the *X-Y-Z* directions.

rates due to their composition, density, and viscosity variations. Hence, for a pair of DIW and VPP materials, the material diffusion effect needs to be characterized to ensure a successful photocuring-while-dispensing process. Here, a strategy to limit the liquid diffusion effect is to quickly cure the dispensed material (or VPP material), before the two materials' diffusion can affect the boundary of the dispensed trace; however, caution must be taken to avoid placing the scanning UV laser spot too close to the dispensing nozzle tip and clogging the tip over the printing process. Note a nozzle to dispense even a nonphotocurable material may still be clogged since the nozzle tip is surrounded by the photocurable matrix material all the time.

We performed a systematic study for a pair of DIW and VPP materials to determine the appropriate delay time between the scanning laser spot and the dispensing nozzle tip. Our designed experiments involve dispensing a straight line of material with a length of 50 mm at a constant moving speed onto the substrate surface. We then use a scanning laser spot with a different delay time to follow the dispensing path and solidify both liquid materials. Various scanning speeds and printing settings were applied to the dispenser, as shown in Figure 2a,b. The specific measurement and data collection methods are illustrated in Figure S5 (Supporting Information). The data collected from the experiments is then used to characterize the diffusion effect, which is assumed to exhibit 1D Fickian diffusion in the dispensed traces inside the liquid matrix material[44]

$$C(x,t) = \frac{N/A}{\sqrt{4\pi Dt}} \exp\left(\frac{-(x-x_0)^2}{4Dt}\right) \quad (1)$$

where C is the dispensed material concentration, N is the number of material molecules, A is the cross-sectional area through which it diffuses, x_0 is the position of the line source along the X-axis, perpendicular to the line length, D is the diffusion constant, and t is the time. The peak width, measured as the temporal peak variance, is first converted to a spatial peak variance (σ^2) and then using the Einstein–Smoluchowski equation

$$\sigma^2 = 2Dt \quad (2)$$

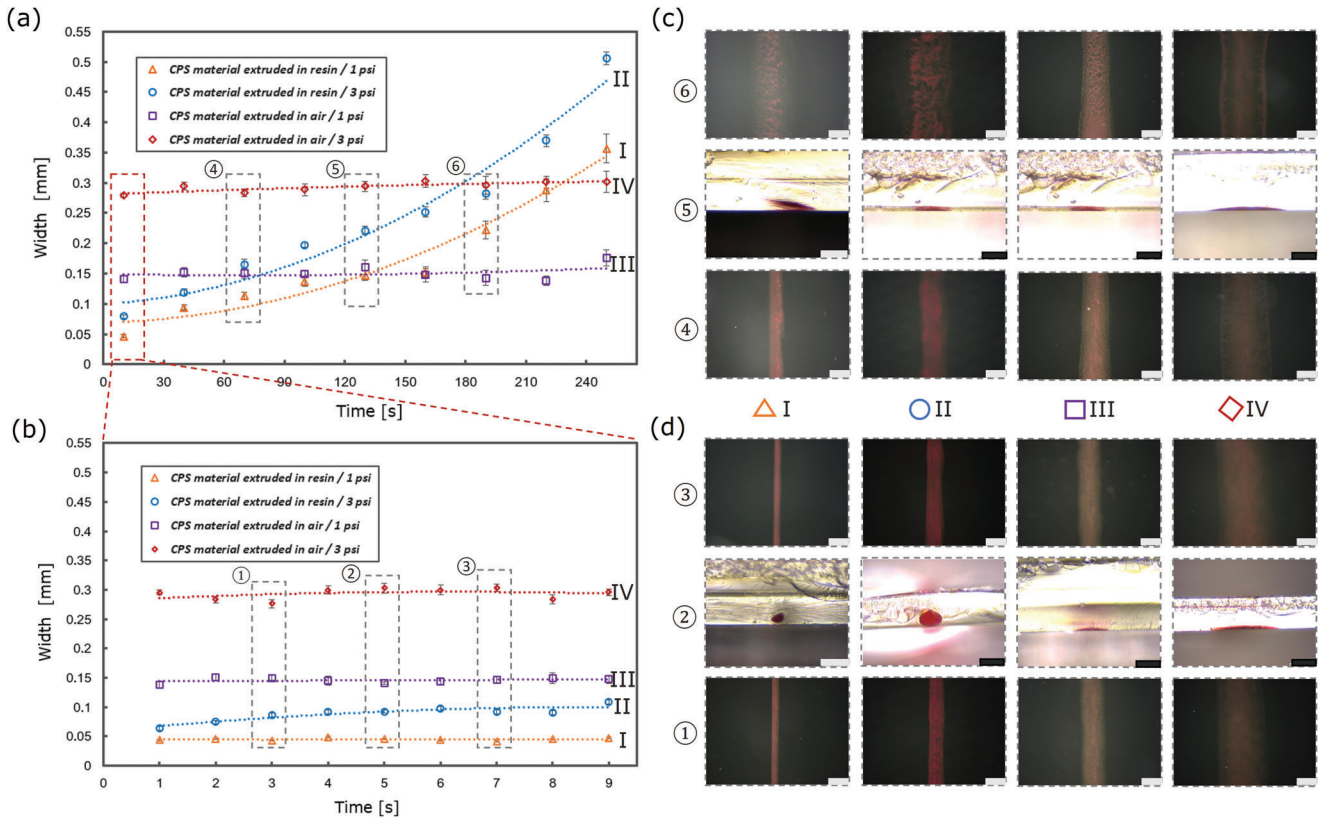

Figure 2. A study of the diffusion effect between the dispensed trace in the air and the matrix material. a) The width of the dispensed trace in the air and liquid resin versus different delay times before photocuring the trace under different printing settings. b) A region of interest in (a), photocure the dispensed trace within a short delay (within 9 s). c) The corresponding microscopic views from samples in (a), groups ④ and ⑥ are the top views of the dispensed traces under different printing settings, group ⑤ is the cross-sectional views of the dispensed traces under different printing settings, all scale bars: 0.1 mm. d) The corresponding microscopic views from samples in (b), group ① and ③ are the top views of the dispensed traces under different printing settings, group ② is the cross-sectional views of the dispensed traces under different printing settings, all scale bars: 0.1 mm.

The above equation can be rewritten as a standard Gaussian function to describe the defusion effect over time

$$C\ (x,t) = \frac{N/A}{\sqrt{2\pi}\sigma}\ \exp\left(\frac{-\left(x-x_0\right)^2}{2\sigma^2}\right) \tag{3}$$

Our measurements reveal several observations about the diffusion effect in the photocuring-while-dispensing process. First, when dispensing in the air, the width of the dispensed material trace remains stable over a long period (over 240 s); in comparison, as time passes after dispensing material in the matrix material, the diffusion between the two liquid materials causes the dispensed trace to increase its width gradually. As shown in Figure 2a, the dashed lines represent the fitted trend of the corresponding data points over different delay time. The top and cross-sectional views of the dispensed traces at six delay moments are shown in Figure 2c,d. Hence, it is critical to photocuring the dispensed material trace before the liquid diffusion can harm the printing results. Second, increasing the air pressure results in a corresponding increase in the width of the dispensed traces in the air and the matrix material (Figure 2a,b). Third, when the same air pressure is applied, the width of the dispensed material trace in the air is about three times wider than that of the dispensed trace in the matrix material (Figure 2b). At the same time, the Z thickness of the dispensed trace in the air is only around 15 and 12 μm for the applied 1 and 3 psi, respectively, after the trace settles down on the substrate surface (Figure 2d). In comparison, the Z thickness of the dispensed trace in the matrix material is around 60 and 80 μm for the applied 1 and 3 psi, respectively (Figure 2d). The width and thickness differences suggest that, when dispensing in the air, the material trace collapses in the Z direction and expands its width as soon as it exits the nozzle tip; in comparison, when dispensing in the matrix material, the surrounding liquid prevents the dispensed trace from collapsing when exiting the nozzle tip due to surface tension.[10,37,38] Hence, the photocuring-while-dispensing strategy could lead to an on-command material deposition with a higher width resolution and a larger Z thickness than the traditional DIW process in the air.

The photocuring-while-dispensing method has another advantage when dispensing photocurable materials using the DIW process. From our experiments, a 500 mW scanning laser cannot fully solidify thin liquid photopolymer traces dispensed in the air due to the oxygen inhibition effect.[45] That is, the oxygen in the air penetrates the liquid photopolymer and consumes the free radicals contained in the liquid resin during the polymerization

process. In comparison, the developed hybrid 3D printing process by immersing the dispenser nozzle tip in the matrix material to dispense the same liquid photopolymer trace naturally prevents the oxygen in the air from penetrating the dispensed material, ensuring the scanning laser with the same laser power to solidify the dispensed material trace more easily.

2.2. Multiexposure Mechanisms for Bonding Between Layers

To access the extruded material with both laser scanning and nozzle dispensing during the printing process, the bottom-up configuration is adopted in printing each layer of a computer-aided design (CAD) model on the substrate film of the vat. The printed layer is then transferred to the previously built layers after all the dispensed materials in the current layer have been fixed on the substrate film surface. Two critical requirements in each layer's fabrication to ensure the multilayer printing process are: 1) the dispensed material from the nozzle tip will be fixed on the substrate film and the current layer will not move when the printing platform with the previously built layers moves down to approach it, and 2) the current layer will securely bond to the previously cured layers to continue the layer-based printing process.

We propose a multiexposure method to address the requirements by considering two circumstances separately. 1) If the DIW material is photocurable similar to the matrix material, we use a double-exposure mechanism to transfer the currently dispensed layer from the bottom film to the previously cured layers, as shown in **Figure 3**a–c. First, a low-power input is given to the laser scanning system, which photocures the dispensed trace on the film surface into a gel-like state during the process, as illustrated in Figure 3a. Next, the printing platform moves down to the current layer position. A second exposure with relatively high energy input is applied to fully cure the current gel-like layer so it can firmly attach to the previously cured layers, as depicted in Figure 3b. The chemical bonding force between the current and previous layers is stronger than the attaching force between the current layer and the substrate film surface, similar to the traditional bottom-up VPP process.[41] Consequently, the printing platform can move up and separate the current layer from the substrate film, as shown in Figure 3c. 2) If the DIW material is nonphotocurable such as electrically conductive ink, liquid metal, or magnetic materials, a triple-exposure mechanism is proposed. First, a thin layer of matrix material is cured by the scanning laser, serving as a bed to hold the nonphotocurable material when detaching from the substrate film. Then, the nonphotocurable material is dispensed onto the surface of the previously cured thin layer. A second laser exposure is applied to cure the matrix material surrounding the nonphotocurable material trace to form a boundary wall in a gel-like state. This boundary wall wraps the nonphotocurable material and confines it within the boundary wall to prevent it from collapsing further. When the printing platform moves down to the current layer position, the geometric shape of the nonphotocurable material can be well-preserved. Finally, a third exposure fully cures the current layer and attaches it to the previously built layers. The printing platform then moves up and separates the current layer from the bottom film. This process is illustrated in Figure 3d–g for 3D printing multifunctional materials. Both photocurable and nonphotocurable materials have been tested using the aforementioned multiexposure method. The shape resolution and layer bonding of the 3D-printed parts for different test cases have also been verified.

2.3. Process Demonstration and Characterization

To demonstrate the effectiveness of the developed hybrid 3D printing process for creating multimaterial objects without material contamination, we first print a 3D ant enclosed in a transparent cuboid inspired by amber in nature.[46] We utilized two photocurable materials with different colors (refer to materials in Section 4) in the designed amber. A 3D digital model (**Figure 4**a) was sliced into multiple 2D layers with a thickness of 100 μm (Figure 4b). Each layer was converted into a G-Code toolpath, as shown in Figure 4c. For the best contour result, a concentric toolpath pattern was selected for this test case. Based on the diffusion study in Section 2.1, a 10 s delay time was implemented in the scanning laser path to account for the diffusion of the dispensed trace. Both the laser scanning and syringe dispensing speeds were set at 10 mm s^{-1}. Prior to carrying out the experiment, a toolpath simulation was performed to ensure the desired target result (Figure 4d).

Once completing all the preparations, we started the printing process by inserting the dispenser needle into a reservoir of the transparent matrix material, ensuring a gap of a layer thickness between the dispenser tip and the bottom surface. A 2D sliced layer is drawn on the substrate surface using the predefined G-Code toolpath. At the same time, a scanning laser spot, with a 10 s delay, follows the dispenser toolpath to cure the dispensed trace in the right place to prevent the diffusion between the two liquid resins (refer to Video S1 in the Supporting Information). After the first exposure, the current 2D layer on the substrate becomes gel-like and sticks to the substrate surface without further diffusion. However, the crosslinked polymer network is not fully finalized, and another exposure is needed for complete polymerization.[47] After all the deposition traces are dispensed and photocured in the desired locations, the current layer is transferred under the lowered building platform and cured with the previously built layers using a second exposure with a higher laser power, as shown in Figure 4i; and Video S2 (Supporting Information).

During the photocuring-while-dispensing 3D printing process, a small amount of matrix material may be left between the current layer and the previously built layers due to the imperfect flatness of the current layer's top surface. When the extruded material exits the dispenser nozzle tip with no constraint, it forms a cylindrical shape; and multiple cylindrical lines overlaying one another form a nonflat plane on the top surface, as shown in Figure 4g. However, as shown in Figure 4f, the bottom surface of the previously cured layers contacts the substrate film in the material reservoir with the same surface quality. Hence the bottom surface of the newly cured layer is flat, defined by the substrate surface (refer to Figure S4c in the Supporting Information for the corresponding SEM image of different substrate surfaces). The liquid matrix material sandwiched between the previously built and current layers also acts as an adhesive to firmly attach the current layer to the previously built layers upon the

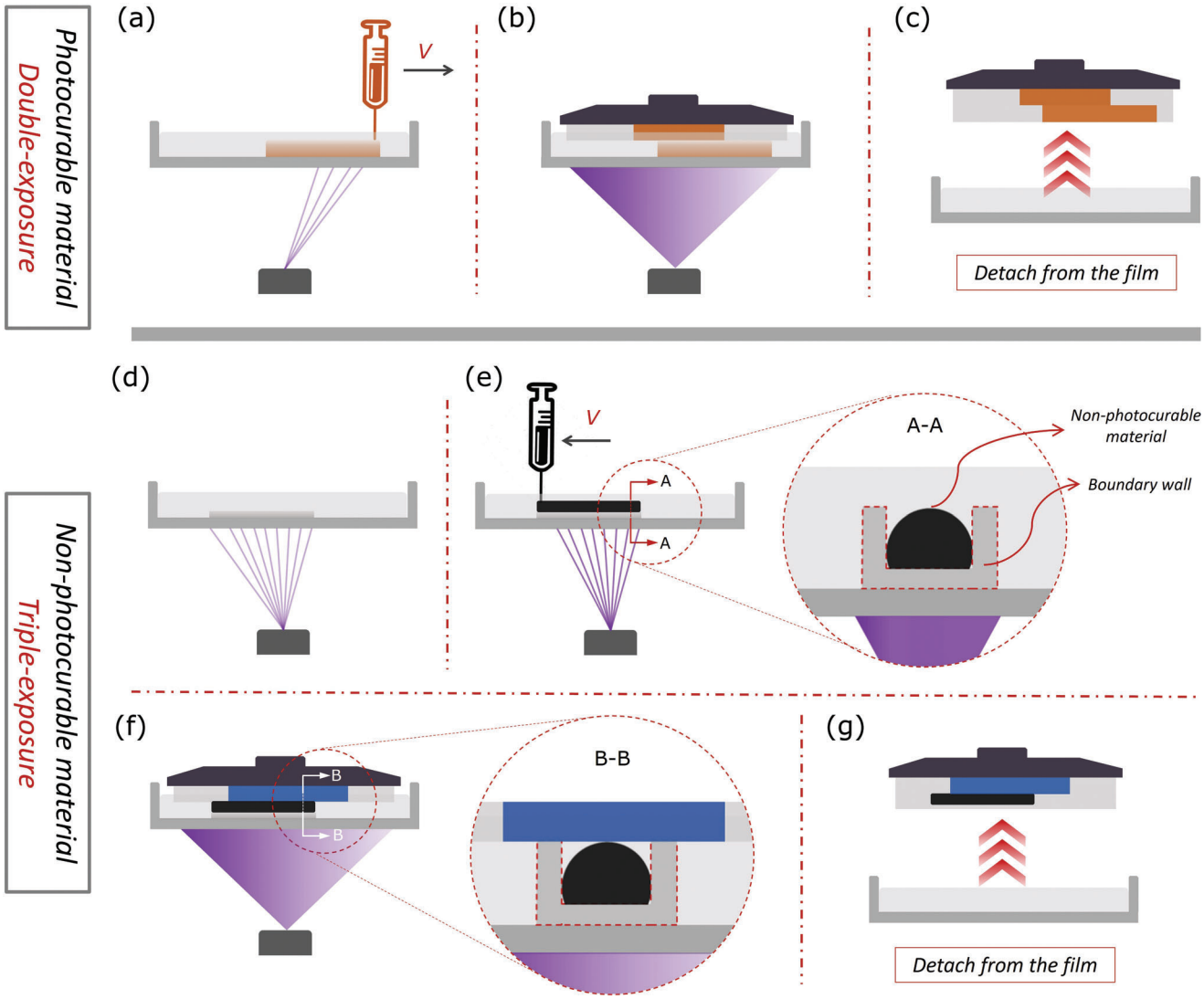

Figure 3. The multiexposure method ensures the bonding between layers. a–c) A double-exposure mechanism is applied when using photocurable materials in multimaterial 3D printing. (a) First, a UV light exposure is applied to photocure the dispensed trace into a gel-like state; b) the printing platform is moved down, and a second exposure is used to fully cure the current layer and attach it to the previously built layers; c) move up the printing platform to detach the built layers from the bottom substrate film. d–g) A triple-exposure mechanism is applied when using non-photocurable materials in multimaterial 3D printing. d) The first exposure is applied to cure a thin layer of matrix material on the bottom film of the reservoir; e) the non-photocurable material is dispensed onto the previous cured thin layer, and a second exposure is applied to generate a gel-like boundary wall around the dispensed trace; f) the printing platform is moved down, and a third exposure is used to fully cure the current layer and attach it to the previously built layers; and g) move up the printing platform to detach the part from the bottom substrate film.

second exposure, as depicted in Figure 4j. In this test case, we have opted to cure a square-shaped matrix material around the 3D ant in each layer to safeguard its delicate structures and support its overhanging structures, as illustrated in Figure 4f. The multilayer fabrication process consists of repeatedly switching between dispensing and photocuring the target material and applying a second exposure to transfer the current layer to the previously built layers, as depicted in Figure 4k. A close-up view of the fabricated result (Figure 4n) demonstrates that small features are well-maintained, indicating the multimaterial printing capability of our method in avoiding material diffusion to preserve printing quality. The side and back views of the fabricated ant are displayed in Figure 4l,m, respectively. A cross-sectional view of the fabricated ant is shown in Figure 4o,p shows the dimensional accuracy of the fabricated ant compared to the input CAD model, which is within ±8%. The method used to measure the dimensional accuracy is described in Figure S5 (Supporting Information).

2.4. Functional Heterogeneous Materials

Functional heterogeneous materials are frequently used in soft robotics, wearable devices, and flexible sensors, to name a

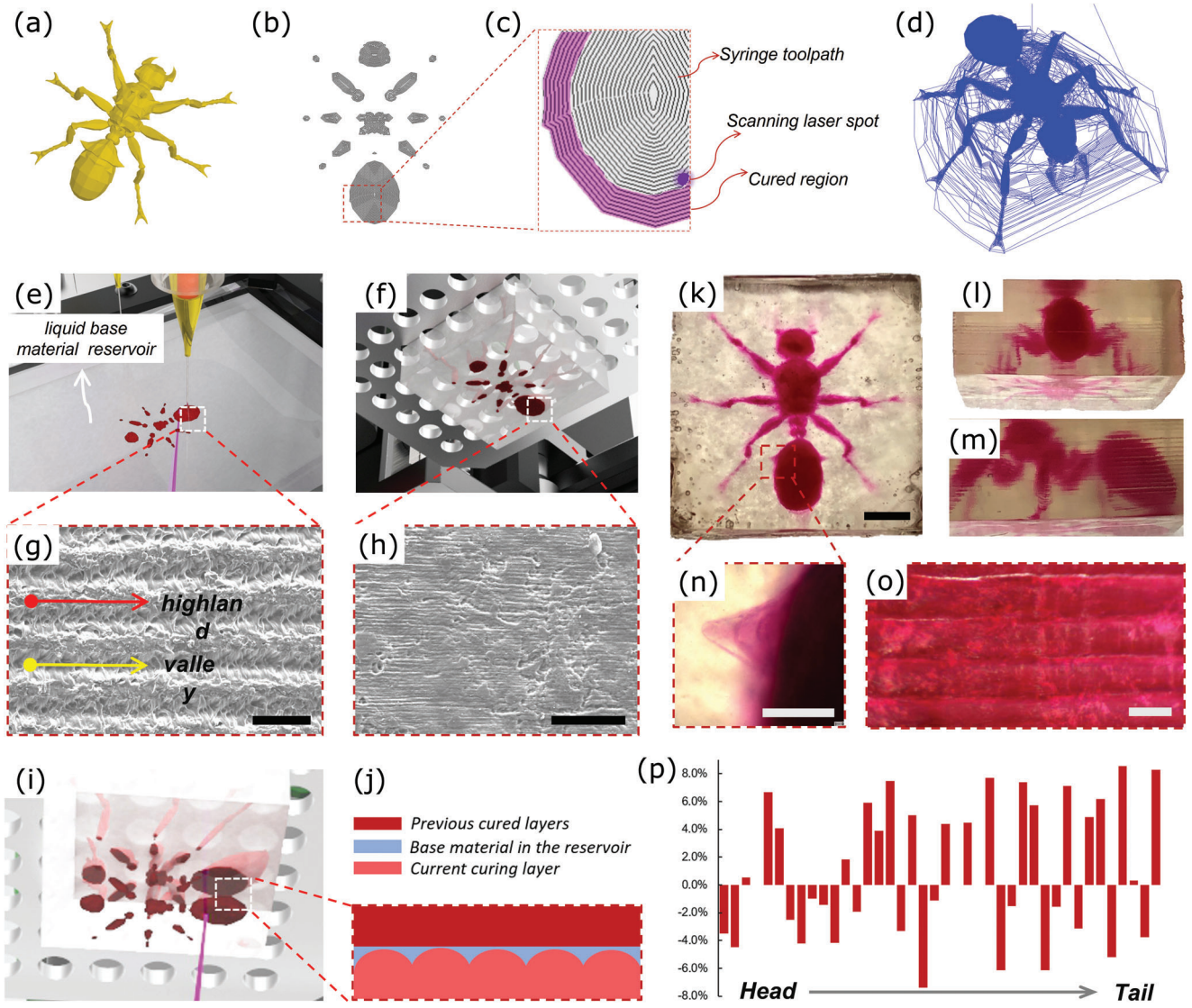

Figure 4. A 3D-printed multimaterial crystal ant in amber. a) Input 3D digital CAD model. b) Sliced layers of the digital model. c) Region of interest in (b), the concentric G-Code syringe toolpath, and the scanning laser path. d) Visualization of the G-Code toolpath. e) Follow the G-Code toolpath to dispense the red resin in the transparent matrix material. The laser spot follows the same toolpath to photocure the dispensed red resin trace. f) Photocured layers stick on the building platform. g) SEM image of the top surface of the newly built layer, scale bar: 0.1 mm. h) SEM image of the bottom surface of the previously built layers, scale bar: 0.1 mm. i) Transfer the newly semicured layer in the material reservoir to the previously built layers using a second exposure by scanning the matrix material in a square shape for this case. j) An illustration of the bonding between the newly cured and previously built layers. k) Top view of the built part, a red ant with surrounding cured transparent resin, scale bar: 5 mm. l) Back view of the built part. m) Side view of the built part. n) Microscopic views of the corresponding detailed features in (k), scale bar: 0.5 mm. o) The cross-sectional view of the built part, scale bar: 0.1 mm. p) The dimensional accuracy of the fabricated ant comparing with the input CAD model.

few. There is increasing interest in 3D printing heterogeneous structures with varying stiffness using photocurable and non-photocurable materials. Our hybrid 3D printing method is especially suitable for a multimaterial part that requires VPP to define the part's complex geometric shape with high accuracy and speed, and use DIW to embed functional materials with simpler shapes to enhance the part's properties. Here we present three multimaterial designs to achieve different functions to illustrate the effectiveness of the developed hybrid 3D printing method.

2.4.1. Functionally Graded Materials

We used the constructed experimental setup to fabricate tensile bars with varying percentages of stiff and soft materials using designed infill patterns to achieve tunable stiffness of the 3D-printed multimaterials. The designed tensile bars incorporate interwoven patterns with different filling rates ranging from 0% to 100%, as illustrated in **Figure 5**a. The stiff interwoven structures embedded within the soft material are expected to enhance the strength of the soft material after solidification. The tensile

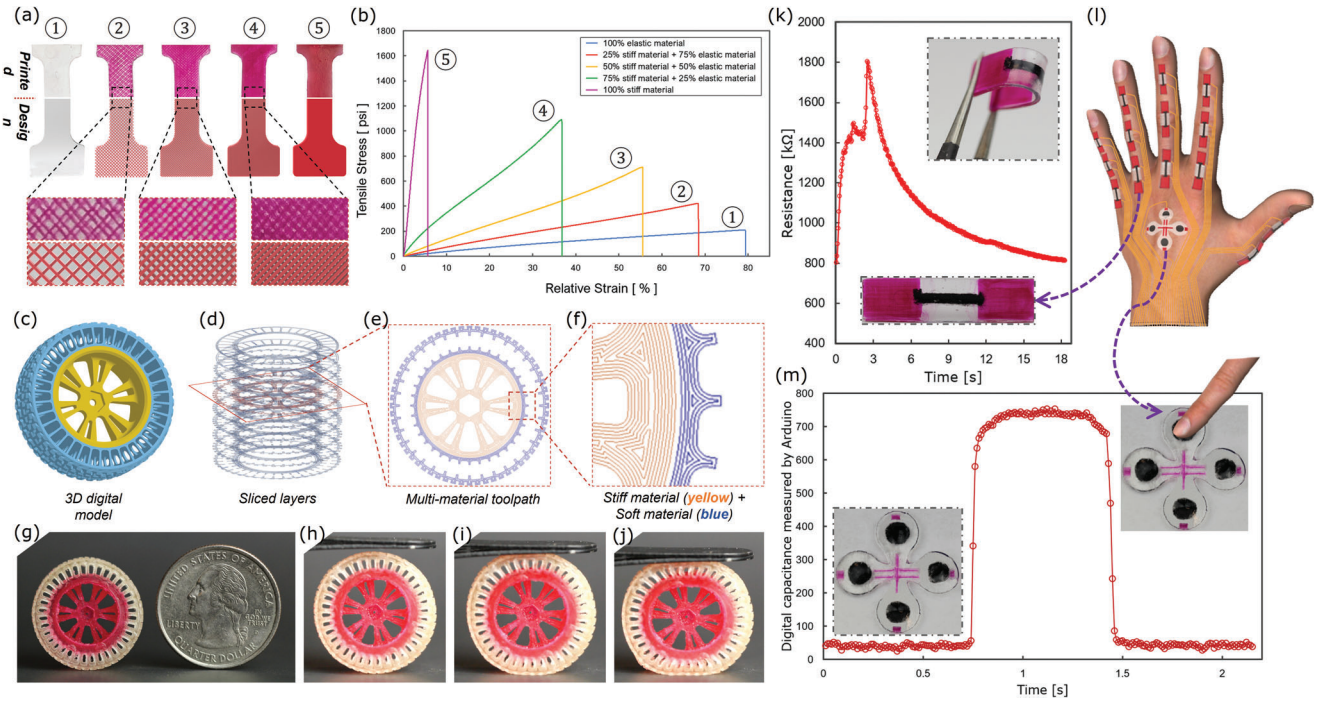

Figure 5. 3D print multimaterial parts with different functionalities. a) Designed tensile bars of varying stiffness using interwoven structures of a stiff DIW material. The red color indicates the rigid material applied, and the grey color suggests the soft/elastic material applied. 0%, 25%, 50%, 75%, and 100% of the stiff material are used correspondingly in the designed tensile bars. b) Corresponding tensile test results for different combinations of soft and rigid materials. c) Input 3D digital CAD model. d) Sliced layers of the digital input model in (c). e) Multimaterial G-Code toolpath. f) Region of interest in (e), the rim is applied with the stiff material, and the tire is applied with the soft material. g) The 3D-printed multimaterial wheel. h–j) The wheel under compression. k) A plot of the resistance change for a strain sensor fabricated by the process. l) Schematic design of the wearable sensors on the human hand. m) A plot of digital capacitance change for a capacitive sensor fabricated by the hybrid 3D printing process.

test results indicate that the stiffness of the designed multimaterial composition can be adjusted using different percentages of stiff materials deposited by DIW and soft materials photocured by VPP, as shown in Figure 5b. The tensile bars' relative strain has a nonlinear relation with the volumetric percentage of the stiff material, with a reduction of the relative strain by half when the stiff material's volumetric percentage increases by 75%. Since different heterogeneous material distributions lead to different mechanical properties, new material properties using other interwoven patterns between the two base materials can be designed and added to the material library.

2.4.2. Integration of Two Photocurable Materials

To showcase the ability to create multimaterial parts with distinct heterogeneous materials, we printed a 3D wheel with materials of different stiffnesses assigned to different regions. The red color in Figure 5g indicates the stiff material assigned to the rim, deposited by a moving dispenser guided by the DIW's G-Code toolpath. The semitransparent material, the soft material assigned to the tire, is the matrix material solidified by the scanning laser at the second exposure stage guided by the laser's G-Code toolpath. The software generates multimaterial G-Code toolpaths for each sliced layer, with varying toolpath for different materials or components. Each material's filling pattern and filling rate can be customized, as shown in Figure 5c–f. We performed a compression test on the 3D-printed wheel, as depicted in Figure 5h–j; and Video S3 (Support Information). The soft material tire deforms significantly under compression, while the stiff rim structure maintains its shape with a much smaller deformation. Since both materials are photocurable resins, the bonding between them, defined by the second laser scanning process discussed in the double-exposure mechanism in Section 2.2, is strong.

2.4.3. Integration of Nonphotocurable and Photocurable Materials

Finally, we tested the hybrid 3D printing process using two photocurable resins (soft and rigid) and a nonphotocurable electrically conductive material to fabricate a wearable device with flexible sensors. Two common types of flexible sensors, the resistance-based strain sensor and the capacitive-based contact sensor, were designed as shown in Figure 5l. The 3D-printed resistance-based strain sensors will be mounted on finger joints to measure their bending angle. The capacitive sensors will be mounted on the dorsal side of the hand, serving as responsive buttons for human–computer interaction. Three types of materials were used in both sensors. The transparent matrix material in the VPP tank is soft, the red DIW material is rigid, and the black DIW material is electrically conductive. The schematic designs of the wearable sensors and their corresponding testing methods are also shown in Figure S8 (Supporting Information). After the printing process, we manually connected the embedded

electrically conductive material with the microcontroller and electric circuits using copper wires (Figure S8 in the Supporting Information). The strain sensor showed a 125% resistance change when the joints were bent (Figure 5k), while the capacitive sensor showed a 14× capacitance change when the buttons were pressed (Figure 5m). A video demonstration of the capacitive sensor can be found in Video S4 (Supporting Information).

3. Discussion and Conclusion

This study reported a novel hybrid 3D printing process combining the deposit-on-demand DIW process with the laser-curing-based VPP process to achieve multimaterial 3D printing. It overcomes the limitations of both AM processes in fabricating heterogeneous structures. The VPP-based 3D printing is limited in its multimaterial printing ability due to resin tank switch and material contamination issues, and the DIW-based 3D printing process struggles with the use of slower mechanical motions to dispense materials from nozzle tips and the maintain of dispensed geometric shapes due to material fluidity. Here the developed hybrid 3D printing process incorporates a photocuring-while-dispensing strategy to address these limitations, resulting in a versatile 3D printing process that can use various materials and build heterogeneous structures with complex shapes and delicate features. The resolution of this hybrid process is largely limited by the nozzle-based DIW process. A conducted diffusion test demonstrates the unique properties and advantages of the liquid-resin-based material dispensing approach over the traditional in-air dispensing, leading to a higher DIW resolution using the same printing parameters. It also shows a safe distance between the dispensing nozzle tip and the scanning laser spot defined in the toolpath planning can avoid the nozzle tip's clogging issue. Several test cases were designed, fabricated, and tested to verify the multiexposure mechanisms and to demonstrate the achievable functionality using this multimaterial 3D printing process.

In the hybrid 3D printing method, it is generally desired to use a photocurable liquid resin with low viscosity as the matrix material and deposit multiple functional materials with a wide range of material properties at any specified 3D space inside the matrix material. In general, a deposited material needs to have a similar or larger density than the matrix material so it will not float up after exiting the nozzle tip. The bottom-up configuration adopted in our setup enables the laser beam's unblocked access to the extruded material traces during the layer printing process, presenting tremendous freedom in optimizing printing parameters for different materials. The hybrid process will significantly expand the material selection of VPP by selectively depositing highly viscous photocurable and nonphotocurable materials. It will also significantly expand the fabrication capability of DIW by using UV light to define geometric shapes and delicate features precisely without mechanical disturbance. In the future, the matrix material can also be photocured first to create the outer shell of a part so the functional materials can be dispensed in the inner region of the part.[34]

With its principle demonstrated, future work will involve implementing an in situ method to synchronize motion between the two AM processes in real-time, reducing toolpath alignment errors and improving dynamic reliability. Another exciting area to explore for the hybrid 3D printing process includes testing the VPP materials that can be chemically dissolved after printing and incorporating more functional DIW materials so the multimaterial 3D printing process could be used to fabricate advanced structures and even integrated devices for biomedical and other applications.

4. Experimental Section

Materials: The materials used in the hybrid multimaterial 3D printing process include Anycubic clear, a UV-curable material purchased from Anycubic (Shenzhen, China). It was used as the matrix material in two test cases. The UV-curable red material, CPS PR57-M, loaded in the DIW dispenser and used in all the experiments, was purchased from Colorado Photopolymer Solutions (CPS, CO). The soft elastic material, Formlabs elastic, used in building the tensile bars, wheel, and wearable sensors, was purchased from Formlabs (MA, USA). The electrically conductive ink, carbon conductive grease, was used in building the wearable sensors and purchased from MG Chemicals (B.C., Canada). All the materials were used as received without modifications. The combinations of the materials in all the test cases and their material properties are shown in Tables S1 and S2 (Supporting Information), respectively.

Selection of the Substrate Film: The surface properties of the substrate film are important in the developed hybrid 3D printing process, and specific criteria need to be met when selecting the appropriate film. First, it should have a reasonable level of light transmission and be chemically compatible with the liquid photopolymers used in the experiments. Second, the dispensed material trace must remain steady on the substrate surface and not bulge due to surface tension, leading to a discontinuous trace. In the experiments, a 0.003″ thickness TPX/Polymethylpentene (PMP) film from CS Hyde (IL, USA) based on pre-experimental tests, as shown in Figure S4 (Supporting Information) was utilized.

Uniaxial Tensile Test: Uniaxial tensile tests were conducted to evaluate the mechanical properties of the 3D-printed tensile bars with varying filling rates of the dispensed stiff material. These tests were performed on an Instron 5492 Dual Column Testing machine at a strain rate of 1 mm min^{-1}. The specimens had dimensions of 15 mm × 4 mm × 0.5 mm. Five samples with the same alignment were tested in all the experiments to minimize potential experimental errors. All the test samples were fabricated using the proposed hybrid 3D printing process and postcured for 15 min in a 60 W ultraviolet (UV) lightbox to ensure complete polymerization before the tensile tests.

Printing Parameters: In the experiments in Figures 4 and 5, a dispenser needle (32 gauge Yellow 0.5" length, VWR International, USA) with an inner diameter of 90 µm for CPS PR57-M was used. The pneumatic pressure applied was 3 psi. In comparison, the conductive ink with a much larger viscosity was dispensed using a conical nozzle tip with an inner diameter of 200 µm under a pneumatic pressure of 6 psi. The constant moving speed of the dispenser in the *XY* direction was 10 mm s^{-1}, and the scanning speed of the laser spot in the *XY* plane was also 10 mm s^{-1} to follow the nozzle movement. The scanning laser spot was delayed 10 s when following the dispensing trace (refer to Video S1 in the Supporting Information). A 405 nm UV laser with a total power of 300 mW was used in the setup, and the diameter of the focused laser spot was 150 µm. The dynamic laser power output was realized by the microcontroller's pulse width modulation (PWM) mechanism, and the printing layer thickness in the experiments was 100 µm. (1) For the double-exposure mechanism, 25% of the full laser power was first used to cure the dispensed CPS PR57-M material in Anycubic clear resin as the matrix material. 60% of the full laser power was used to cure the dispensed CPS PR57-M material when using Formlabs elastic resin as the matrix material, since Anycubic clear resin has a much larger cure depth than Formlabs elastic resin for the same light energy input. After the current layer was transferred from the substrate surface to the previously solidified layers, 80% of the full laser power in the second exposure stage was applied. 2) For the triple-exposure mechanism, the printing process involved using 40% of the full laser power for the initial exposure to cure the matrix material to form a base layer with

a thickness of around 20 µm, allowing the conductive ink to be applied in the subsequent step. For the second exposure, 60% of the full laser power was used to cure the neighboring matrix material around the trace; finally, 80% of the full laser power in the layer transferring step was used to bond with the previously built layers. The amount of energy input during different stages was precalibrated to meet the desired curing depth and width requirements. The detailed modeling of the hybrid 3D printing process is shown in Figure S2 (Supporting Information).

Multimaterial Slicer: To slice the multimaterial 3D digital model, the open-source software Sli3r, which allows assigning different material profiles to various individual components associated with different dispensers was used. The concentric filling pattern for the 3D ant model, the 3D wheel model, and the capacitive buttons, as shown in Figure 4 and Figure 5c,m, respectively, was chosen. The linear filling pattern for the tensile test cases and the strain sensor, as shown in Figure 5a,k, respectively, was chosen. A Python script was written to modify the G-Code toolpath generated by Sli3r, encoding customized actuation information for the low-level main controller to decode and drive additional general-purpose input/output (GPIO) controlled actuators associated with the linear motion movement and dispensing events.

Motion Synchronization: The movements of the dispensing and laser scanning systems must be synchronized to ensure the successful implementation of the proposed hybrid 3D printing process. For two initially independent AM systems, it is crucial to calibrate the spatial coordinates between them before printing to avoid any misalignment of the dispensers and the laser scanning spot. Similarly, coordinates calibration must be carried out between different dispensers. A simple image recognition method was used to adjust the transformation matrix applied to the generated G-Code to align their coordinates (refer to Figure S3 in the Supporting Information). Moreover, SEM images of dispensed layers and substrate films provide insights into the surface morphology and microstructure of the samples.

Supporting Information

Supporting Information is available from the Wiley Online Library or from the author.

Acknowledgements

The authors acknowledged the support from National Science Foundation (NSF) (Grant No. 1663663). The authors acknowledged the Center for Electron Microscopy and Microanalysis at USC for the SEM images, and Prof. Qiming Wang and Dr. Kunhao Yu at USC for their help with the mechanical tests.

Conflict of Interest

The authors declare no conflict of interest.

Author Contributions

Y.C. and J.J. initiate the idea. J.J. designed the hybrid 3D printing system. F.Z. and Y.Y. did some of the experiments. F.Z. designed test cases for experiments. C.Z. did simulation work for the experiments. Y.Y. and H.W. studied materials used for the hybrid process. J.J. and Y.C. wrote the manuscript.

Data Availability Statement

The data that support the findings of this study are available in the Supporting Information of this article.

Keywords

composite materials, direct ink writing, hybrid printing, multimaterial, stereolithography

Published online:

[1] X. Wang, M. Jiang, Z. Zhou, J. Gou, D. Hui, *Composites, Part B* **2017**, *110*, 442.
[2] Y. Yang, Z. Chen, X. Song, Z. Zhang, J. Zhang, K. K. Shung, Q. Zhou, Y. Chen, *Adv. Mater.* **2017**, *29*, 11.
[3] Y. Yang, X. Li, M. Chu, H. Sun, J. Jin, K. Yu, Q. Wang, Q. Zhou, Y. Chen, *Sci. Adv.* **2019**, *5*, 4.
[4] S. J. Leigh, R. J. Bradley, C. P. Purssell, D. R. Billson, D. A. Hutchins, *PLoS One* **2012**, *7*, 11.
[5] X. Wei, D. Li, W. Jiang, Z. Gu, X. Wang, Z. Zhang, Z. Sun, *Sci. Rep.* **2015**, *5*, 11181.
[6] S. Bose, S. Vahabzadeh, A. Bandyopadhyay, *Mater. Today* **2013**, *16*, 496.
[7] H. N. Chia, B. M. Wu, *J. Biol. Eng.* **2015**, *9*, 4.
[8] B. N. Peele, T. J. Wallin, H. Zhao, R. F. Shepherd, *Bioinspir. Biomim.* **2015**, *10*, 055003.
[9] M. Wehner, R. L. Truby, D. J. Fitzgerald, B. Mosadegh, G. M. Whitesides, J. A. Lewis, R. J. Wood, *Nature* **2016**, *536*, 451.
[10] J. T. Muth, D. M. Vogt, R. L. Truby, Y. Mengüç, D. B. Kolesky, R. J. Wood, J. A. Lewis, *Adv. Mater.* **2014**, *26*, 36.
[11] A. D. Valentine, T. A. Busbee, J. W. Boley, J. R. Raney, A. Chortos, A. Kotikian, J. D. Berrigan, M. F. Durstock, J. A. Lewis, *Adv. Mater.* **2017**, *29*, 1703817.
[12] Y. Yang, X. Song, X. Li, Z. Chen, C. Zhou, Q. Zhou, Y. Chen, *Adv. Mater.* **2018**, *30*, 36.
[13] Y. Leung, T. Kwok, X. Li, Y. Yang, C. Wang, Y. Chen, *J. Comput. Inf. Sci. Eng.* **2019**, *19*, 021013.
[14] H. Yang, J. C. Lim, Y. Liu, X. Qi, Y. L. Yap, V. Dikshit, W. Y. Yeong, J. Wei, *Virtual Phys. Prototyp.* **2017**, *12*, 1, 95.
[15] S. C. Ligon, R. Liska, J. r. Stampfl, M. Gurr, R. Mülhaupt, *Chem. Rev.* **2017**, *117*, 10212.
[16] D. Chimene, K. K. Lennox, R. R. Kaunas, A. K. Gaharwar, *Ann. Biomed. Eng.* **2016**, *44*, 2090.
[17] M. Guvendiren, J. Molde, R. M. Soares, J. Kohn, *ACS Biomater. Sci. Eng.* **2016**, *2*, 1679.
[18] J. W. Boley, E. L. White, G. T. C. Chiu, R. K. Kramer, *Adv. Funct. Mater.* **2014**, *24*, 23.
[19] M. A. Skylar-Scott, S. Gunasekaran, J. A. Lewis, *Proc. Natl. Acad. Sci. USA* **2016**, *113*, 6137.
[20] B. Chen, Y. Jiang, X. Tang, Y. Pan, S. Hu, *ACS Appl. Mater. Interfaces* **2017**, *9*, 34.
[21] D. Kokkinis, M. Schaffner, A. R. Studart, *Nat. Commun.* **2015**, *6*, 8643.
[22] Y. Kim, H. Yuk, R. Zhao, S. A. Chester, X. Zhao, *Nature* **2018**, *558*, 274.
[23] X. Liu, H. Yuk, S. Lin, G. A. Parada, T. C. Tang, E. Tham, C. de la Fuente-Nunez, T. K. Lu, X. Zhao, *Adv. Mater.* **2018**, *30*, 4.
[24] C. Xu, B. Quinn, L. L. Lebel, D. Therriault, G. L'Espérance, *ACS Appl. Mater. Interfaces* **2019**, *11*, 8.
[25] M. A. Skylar-Scott, J. Mueller, C. W. Visser, J. A. Lewis, *Nature* **2019**, *575*, 330.
[26] J. O. Hardin, T. J. Ober, A. D. Valentine, J. A. Lewis, *Adv. Mater.* **2015**, *27*, 21.
[27] W. Liu, Y. S. Zhang, M. A. Heinrich, F. De Ferrari, H. L. Jang, S. M. Bakht, M. M. Alvarez, J. Yang, Y. C. Li, G. Trujillo-de Santiago, *Adv. Mater.* **2017**, *29*, 3.
[28] Y. Li, H. Mao, P. Hu, M. Hermes, H. Lim, J. Yoon, M. Luhar, Y. Chen, W. Wu, *Adv. Mater. Technol.* **2019**, *4*, 1800638.

[29] Y. Xu, H. Mao, C. Liu, Z. Du, W. Yan, Z. Yang, J. Partanen, Y. Chen, *Small* **2023**, *19*, 2205784.
[30] C. Zhou, Y. Chen, Z. Yang, B. Khoshnevis, *Rapid Prototyp. J.* **2013**, *19*, 153.
[31] D. Han, C. Yang, N. X. Fang, H. Lee, *Addit. Manuf.* **2019**, *27*, 606.
[32] C.-D. Matte, M. Pearson, F. Trottier-Cournoyer, A. Dafoe, T. H. Kwok, *Rapid Prototyp. J.* **2019**, *25*, 864.
[33] H. Mao, W. Jia, Y. Leung, J. Jin, Y. Chen, *Rapid Prototyp. J.* **2021**, *27*, 861.
[34] D. A. Rau, M. Forgiarini, C. Williams, *Addit. Manuf.* **2021**, *42*, 101996.
[35] X. Peng, X. Kuang, D. J. Roach, Y. Wang, C. M. Hamel, C. Lu, H. J. Qi, *Addit. Manuf.* **2021**, *40*, 101911.
[36] X. Peng, S. Wu, X. Sun, L. Yue, S. M. Montgomery, F. Demoly, K. Zhou, R. Zhao, H. J. Qi, *Adv. Mater.* **2022**, *34*, 39.
[37] W. Wu, A. DeConinck, J. A. Lewis, *Adv. Mater.* **2011**, *23*, 24.
[38] C. B. Highley, C. B. Rodell, J. A. Burdick, *Adv. Mater.* **2015**, *27*, 5075.
[39] T. Uchida, H. Onoe, *Micromachines* **2019**, *10*, 433.
[40] T. Bhattacharjee, S. M. Zehnder, K. G. Rowe, S. Jain, R. M. Nixon, W. G. Sawyer, T. E. Angelini, *Sci. Adv.* **2015**, *1*, 8.
[41] W. Jia, Y. Leung, H. Mao, H. Xu, C. Zhou, Y. Chen, *J. Manuf. Sci. Eng.* **2022**, *144*, 3.
[42] R. Karyappa, T. Ching, M. Hashimoto, *ACS Appl. Mater. Interfaces* **2020**, *12*, 23565.
[43] M. Alruwaili, J. A. Lopez, K. McCarthy, E. G. Reynaud, B. J. Rodriguez, *Bio-Design Manuf.* **2019**, *2*, 172.
[44] C. T. Culbertson, S. C. Jacobson, J. M. Ramsey, *Talanta* **2002**, *56*, 365.
[45] J. R. Tumbleston, D. Shirvanyants, N. Ermoshkin, R. Janusziewicz, A. R. Johnson, D. Kelly, K. Chen, R. Pinschmidt, J. P. Rolland, A. Ermoshkin, *Science* **2015**, *347*, 1349.
[46] J. Jin, Y. Chen, *J. Manuf. Proc.* **2017**, *28*, 541.
[47] M. Rubinstein, R. H. Colby, *Polymer Physics*, Oxford University Press, New York **2003**.